# Surface electromagnetic waves in Fibonacci superlattices: theoretical and experimental results

Y. El Hassouani, H. Aynaou, E.H. El Boudouti, Bahram Djafari-Rouhani, Abdellatif Akjouj, V.R. Velasco

# Surface electromagnetic waves in Fibonacci superlattices: Theoretical and experimental results

Y. El Hassouani,[1] H. Aynaou,[1] E. H. El Boudouti,[1,*] B. Djafari-Rouhani,[2] A. Akjouj,[2] and V. R. Velasco[3]
[1]*Laboratoire de Dynamique et d'Optique des Matériaux, Département de Physique, Faculté des Sciences, Université Mohamed Premier, 60000 Oujda, Morocco*
[2]*Institut d'Électronique, de Microélectronique et de Nanotechnologie (IEMN), UMR CNRS 8520, UFR de Physique, Universit de Lille 1, 59655 Villeneuve d'Ascq, France*
[3]*Instituto de Ciencia de Materiales de Madrid, CSIC, Sor Juana Inés de la Cruz 3, 28049 Madrid, Spain*
(Received 15 March 2006; revised manuscript received 18 May 2006; published 13 July 2006)

We study theoretically and experimentally the existence and behavior of the localized surface modes in one-dimensional (1D) quasiperiodic photonic band gap structures. These structures are made of segments and loops arranged according to a Fibonacci sequence. The experiments are carried out by using coaxial cables in the frequency region of a few tens of MHz. We consider 1D periodic structures (superlattice) where each cell is a well-defined Fibonacci generation. In these structures, we generalize a theoretical rule on the surface modes, namely when one considers two semi-infinite superlattices obtained by the cleavage of an infinite superlattice, it exists exactly one surface mode in each gap. This mode is localized on the surface either of one or the other semi-infinite superlattice. We discuss the existence of various types of surface modes and their spatial localization. The experimental observation of these modes is carried out by measuring the transmission through a guide along which a finite superlattice (i.e., constituted of a finite number of quasiperiodic cells) is grafted vertically. The surface modes appear as maxima of the transmission spectrum. These experiments are in good agreement with the theoretical model based on the formalism of the Green function.

DOI: 10.1103/PhysRevB.74.035314 PACS number(s): 41.20.Jb, 77.84.Lf

## I. INTRODUCTION

Photonic crystals (PC) have been a subject of great interest during the last decade because of their interesting properties in the development of new optical circuits.[1,2] These systems, constituted by periodic arrangements (cells) of dielectric materials according to one (1D), two (2D), and three (3D) dimensions, present characteristic areas in the dispersion curves where light can propagate (bulk bands) and areas where light cannot propagate (gaps). These structures present unusual properties which can be exploited in the control and the guidance of the propagation of light.[3] However, in real materials, the photonic crystals are often of finite size with free surfaces. Consequently, the surface modes can exist inside the gaps[4–8] as defect modes. The existence of surface modes can directly affect the performance and the efficiency of PC to prohibit the propagation of electromagnetic waves in certain frequency regions.[4,6] Therefore it is interesting to study surface modes in PC. The study of surface electromagnetic waves in 1D multilayer PC (or superlattice) was largely developed both theoretically and experimentally.[7–17] In particular, it was shown that surface waves in PC can present an alternative to surface plasmons which are typical with metal films. From the technological point of view, surface electromagnetic waves can present some applications in the design of optical devices such as sensors and modulators.[13–17]

Photonic quasicrystals (PQC) are intermediate structures between periodic and disordered systems.[18] The study of the propagation and the localization of light in 1D PQC was largely developed during the last decade.[18–28] Most of these results concern the bulk properties of these structures, however, the study of surface modes has attracted less interest[18] in particular from the experimental point of view. In a recent paper[29] we have briefly studied surface states in 1D photonic band gap structures composed of a waveguide, along which dangling side branches are grafted periodically. In this paper, we focus on the study of the existence and the localization of surface electromagnetic waves in quasiperiodic structures formed by two blocks *A* (segment) and *B* (loop) (Fig. 1) arranged according to the Fibonacci sequence. In particular, we study the surface waves in periodic superlattices where each cell is formed by loops and segments following the Fibonacci sequence. Our objective is threefold: (i) We generalize to the case of quasiperiodic structures a rule about the existence of surface modes, namely, when one considers two semi-infinite superlattices obtained by the cleavage of an infinite superlattice, there is exactly a surface mode in each gap. This mode is localized on the surface of one of the two semi-infinite superlattices. We show that these surface modes correspond to the modes of a single cell when their frequencies fall inside the gaps of the infinite superlattice. (ii) We show that in addition to the existence of surface modes re-

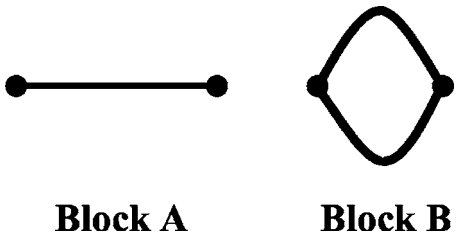


FIG. 1. Schematic representation of the blocks *A* and *B* constituting the Fibonacci structure. The block *A* is a simple coaxial cable of length $d=1$ *m* and impedance $Z=50\ \Omega$. The block *B* is a symmetrical loop made up of two identical coaxial cables of the same length $d=1$ *m* and of impedance $Z=50\ \Omega$.

 

lated to the periodicity as in usual superlattices, there exists new surface modes related to the quasiperiodicity of the loops and segments inside each cell. (iii) We propose an experimental method to observe these surface modes. However, before dealing with surface waves, it is helpful to discuss the band gap structures of infinite Fibonacci superlattices and some related properties. This paper is organized as follows: In Sec. II, we give a short summary of the theoretical formalism and the main analytical results used in our numerical calculations. Section III gives the principal numerical and experimental results about bulk and surface modes. The conclusions are summarized in Sec. IV.

## II. METHOD OF THEORETICAL AND NUMERICAL CALCULATION

The Fibonacci superlattice is a simple periodic 1D structure where each unit cell is constituted by a quasiperiodic structure built of two blocks $A$ and $B$. For the structure considered here, the block $A$ is formed by a simple coaxial cable of length $d=1$ m characterized by its characteristic impedance $Z=50\ \Omega$ and its permittivity $\varepsilon=2.3$, while the block $B$ is a symmetrical loop formed by two identical standard coaxial cables of the same length $d=1$ m (Fig. 1). It is easy to show that each block $B$ (loop) is equivalent to a coaxial cable of length $d=1$ m and characterized by a half impedance $Z/2=25\ \Omega$. This contrast between the characteristic impedances of the two blocks $A$ and $B$ gives rise to the opening of large gaps in the band structure of these serial loop structures.[30,31] The blocks $A$ and $B$ inside each cell of the superlattice follow the Fibonacci sequence:

$$S_{k+1} = S_k S_{k-1} \text{ with } S_1 = [A], \quad S_2 = [AB]. \tag{1}$$

Consequently, the Fibonacci generations are: $S_1=[A]$, $S_2=[AB]$, $S_3=[ABA]$, $S_4=[ABAAB]$, $S_5=[ABAABABA]$,…. The theoretical formalism used is based on the interface response theory.[32] In Ref. 33 El Boudouti *et al.* presented the analytical expressions of the dispersion relations of surface and interface transverse elastic waves in $N$-layer periodic superlattices, i.e., a superlattice in which each cell is composed of $N$ different layers. The expressions of the displacement fields and the local and total densities of states are also given. These expressions also remain valid to study the wave propagation in coaxial cables which are monomode circuits;[34] it is sufficient to replace the acoustic impedances by the electromagnetic impedances and the elastic constants by the dielectric permittivities. The calculation of the Green functions of $N$-layer superlattice [Fig. 2(a)] can be carried out by using the $2\times 2$ transfer matrix:

$$T_{1,\ldots,N} = \Delta_N \Delta_{N-1} \cdots \Delta_1, \tag{2}$$

where

$$\Delta_i = \begin{pmatrix} C_i & -jZ_i S_i \\ \dfrac{jS_i}{Z_i} & C_i \end{pmatrix}, \tag{3}$$

$S_i=\sinh(\alpha_i d_i)$ and $C_i=\cosh(\alpha_i d_i)$. $\alpha_i=\frac{-j\omega\sqrt{\varepsilon_i}}{c}$, $j=\sqrt{-1}$, $\omega$ is the pulsation, $\varepsilon_i$ the dielectric permittivity of the medium $i$, and

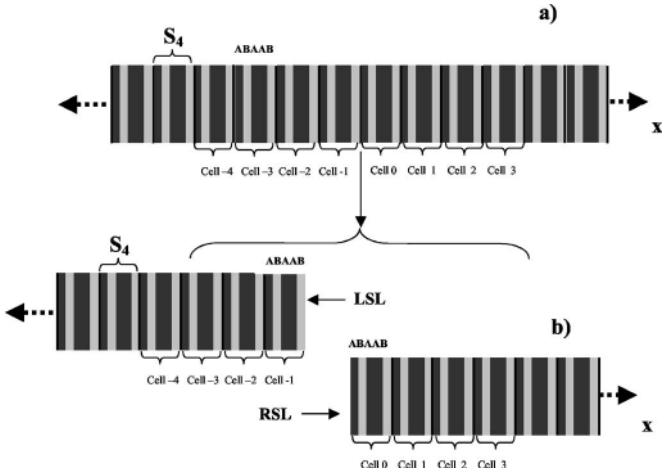


FIG. 2. a) Schematic representation of an infinite periodic superlattice where each cell is composed of a Fibonacci generation (for example, $S_4$). (b) Schematic representation of two semi-infinite superlattices obtained by the cleavage of the infinite superlattice. We notice *RSL* and *LSL* the right-hand side and the left-hand side superlattices.

$c$ the speed of light. In our case, the blocks $A$ and $B$ are characterized by $\varepsilon_A=\varepsilon_B=2.3$ and $Z_A=2Z_B=50\ \Omega$ and the $N$ layers (blocks) inside each cell respect the Fibonacci sequence [Fig. 2(a)]. Consequently, the transfer matrices become [Eq. (2)]: $T^{(1)}=\Delta_A$ for $S_1$, $T^{(2)}=\Delta_B\Delta_A$ for $S_2$, $T^{(3)}=\Delta_A\Delta_B\Delta_A$ for $S_3$, $T^{(4)}=\Delta_B\Delta_A\Delta_A\Delta_B\Delta_A$ for $S_4$,…. Then, a recurrence relation is obtained: $T^{(k+1)}=T^{(k)}T^{(k-1)}$ from which all the matrices $T^{(k)}$ can be obtained where $k$ is the number of the Fibonacci generation. The number of the blocks in each generation $k$ is $F_k=F_{k-1}+F_{k-2}$ with $F_1=1$ and $F_2=2$. Let us notice also the useful property of the transfer matrix valid for any generation number $k$:

$$\det T^{(k)} = T_{11}T_{22} - T_{12}T_{21} = 1, \tag{4}$$

where $T_{11}$, $T_{12}$, $T_{21}$, and $T_{22}$ are the elements of the transfer matrix $T^{(k)}$ [Eq. (2)].

### A. Dispersion relations and Green functions

The dispersion relation of an infinite superlattice (i.e., $\omega$ as a function of the wave vector $Q$), is given by[33]

$$\cos(QD) = \frac{1}{2}(T_{11} + T_{22}) = \eta, \tag{5}$$

where $D=F_k$ (in meters) is the period of the superlattice. Each period is a Fibonacci sequence of order $k$. The calculation of the elements of the Green function $g(DD)$ in the whole space of the superlattice requires first the knowledge of the elements $g(M_mM_m)$ in the restricted space of the interfaces $M_m$ [the index $m$ indicates the block $i$ belonging to the cell $n$: $m\equiv(n,i)$ and $M_m$ represent the space of the two interfaces of the block $i$: $M_m=\left(n,i,\pm\frac{d_i}{2}\right)$, $i=1,2,\ldots,N$]. These elements are given by[33]

$$g\left(n,i,-\frac{d_i}{2};n',j,-\frac{d_j}{2}\right)=\begin{cases}(T_{12})_{i,\ldots,N,1,\ldots,i-1}\dfrac{t^{|n-n'|+1}}{t^2-1}, & i=j,\\ (T_{12})_{j,\ldots,N,1,\ldots,i-1}\dfrac{t^{|n-n'|+1}}{t^2-1}+(T_{12})_{i,\ldots,j-1}\dfrac{t^{|n-n'-1|+1}}{t^2-1}, & i<j\leqslant N,\\ (T_{12})_{i,\ldots,N,1,\ldots,j-1}\dfrac{t^{|n-n'|+1}}{t^2-1}+(T_{12})_{j,\ldots,i-1}\dfrac{t^{|n-n'+1|+1}}{t^2-1}, & j<i\leqslant N.\end{cases} \tag{6}$$

Here the different terms $(T_{12})$ are obtained from Eq. (2) with due account of the indices giving the order of the blocks beginning from the first and ending by the last and $t$ is defined by

$$t=\begin{cases}\eta+(\eta^2-1)^{1/2}, & \eta<-1,\\ \eta\pm i(1-\eta^2)^{1/2}, & -1<\eta<+1,\\ \eta-(\eta^2-1)^{1/2}, & \eta>1.\end{cases} \tag{7}$$

Inside the bulk bands $(-1<\eta<+1)$, the sign $\pm$ in the expression of $t$ has to be chosen such that $|t(\omega^2+i\varepsilon)|_{\varepsilon\to 0}$ will be slightly smaller than one. The expression of the Green function between any two points of the infinite superlattice is given by[33]

$$\begin{aligned}g(n,i,x;n',i',x')=&\,\delta_{nn'}\delta_{ii'}U_i(x,x')\\&+\frac{1}{S_iS_i'}\left\{\sinh\left[\alpha_i\left(\frac{d_i}{2}-x\right)\right];\right.\\&\left.\sinh\left[\alpha_i\left(\frac{d_i}{2}+x\right)\right]\right\}g(M_m,M_{m'})\\&\times\begin{Bmatrix}\sinh\left[\alpha_{i'}\left(\dfrac{d_{i'}}{2}-x'\right)\right]\\ \sinh\left[\alpha_{i'}\left(\dfrac{d_{i'}}{2}+x'\right)\right]\end{Bmatrix},\end{aligned} \tag{8}$$

where

$$\begin{aligned}U_i(x,x')=&-\frac{1}{2F_i}\exp[-\alpha_i|x-x'|]+\frac{1}{2F_iS_i}\\&\times\left\{\sinh\left[\alpha_i\left(\frac{d_i}{2}-x'\right)\right]\exp\left[-\alpha_i\left(\frac{d_i}{2}+x\right)\right]\right.\\&\left.+\sinh\left[\alpha_i\left(\frac{d_i}{2}+x'\right)\right]\exp\left[-\alpha_i\left(\frac{d_i}{2}-x\right)\right]\right\}.\end{aligned} \tag{9}$$

In Eq. (8) the last three terms are the product of a $(1\times 2)$ matrix by the $(2\times 2)g(M_m,M_{m'})$ matrix and by a $(2\times 1)$ matrix. $g(M_m,M_{m'})$ is the $(2\times 2)$ matrix formed out of the elements given by Eq. (6), for $m\equiv\left(n,i,\pm\frac{d_i}{2}\right)$ and $m'\equiv\left(n',i',\pm\frac{d_i'}{2}\right)$. Now, by cutting an infinite superlattice between two cells, one obtains two semi-infinite superlattices. We shall call them left superlattice (*LSL*) and right superlattice (*RSL*) [Fig. 2(b)]. The dispersion relation of a semi-infinite superlattice with free surface [Fig. 2(b)] is given by

$$T_{21}=0, \tag{10}$$

where $T_{21}$ is given by Eq. (2), together with the condition

$$|T_{22}|>1(|T_{22}|<1)\quad \text{for the } RSL\ (LSL). \tag{11}$$

This last condition ensures that the wave is decaying when penetrating into the superlattice far from the surface. The Green function in the space of the interfaces of the semi-infinite superlattice is given by[33]

$$d\left(n,i,-\frac{d_i}{2};n,j,-\frac{d_j}{2}\right)=g\left(n,i,-\frac{d_i}{2};n,j,-\frac{d_j}{2}\right)+\frac{t^{n+n'+1}}{t^2-1}\frac{Y_iY_j}{T_{21}}, \tag{12}$$

where $Y_1=T_{22}$ for $i=1$, and $Y_i=-t(T_{11})_{1,\ldots,i-1}+(T_{22})_{i,\ldots,N}$ for $i=2,\ldots,N$.

The Green function in the whole space of the semi-infinite superlattice is given by Eq. (8) by replacing $g(M_n,M_{n'})$ [Eq. (6)] by $d(M_n,M_{n'})$ [Eq. (12)].

### B. Density of states and displacement fields

The local density of states at a point $x$ of the structure is given by

$$n(\omega;n,i,x)=-\frac{1}{\pi}\operatorname{Im} d^+(\omega;n,i,x;n,i,x), \tag{13}$$

where $d^+(\omega)=\lim_{\varepsilon\to 0}d(\omega+i\varepsilon)$. The total density of states is obtained by integrating over $x$ and summing on $n$ and $i$ the local density of states. We are particularly interested in the total density of states of the semi-infinite superlattice [Fig. 2(b)] from which the contribution of the infinite superlattice is substrated [Fig. 2(a)].

This variation $\Delta_n(\omega)$ can be written as the sum of the variations of the densities of states $\Delta_i n(\omega)$ in any block $i$ of the superlattice:

$$\Delta n(\omega)=\sum_{i=1}^{N}\Delta_i n(\omega), \tag{14}$$

where

$$\Delta_i n(\omega) = -\frac{Z_i}{\pi}\mathrm{Im}\sum_{n=0}^{+\infty}\int_{-d_i/2}^{d_i/2}[d(n,i,x;n,i,x) - g(n,i,x;n,i,x)]dx, \tag{15}$$

$d$ and $g$ are the Green functions of the semi-infinite and the infinite superlattice, respectively. By replacing $d$ and $g$ by their respective values, one obtains:

$$\Delta_i(\omega) = \frac{Z_i\omega}{\pi}\mathrm{Im}\frac{t}{(t^2-1)^2}\left(\frac{1}{\alpha_i S_i^2 T_{21}}\right)[(Y_i^2 + Y_{i+1}^2)(C_i S_i - \alpha_i d_i) + 2Y_i Y_{i+1}(\alpha_i d_i C_i - S_i)], \quad i = 1,2,\ldots,N-1, \tag{16}$$

$$\Delta_N(\omega) = \frac{Z_N\omega}{\pi}\mathrm{Im}\frac{t}{(t^2-1)^2}\left(\frac{1}{\alpha_N S_N^2 T_{21}}\right)\{[Y_N^2 + (tY_1)^2] \times (C_N S_N - \alpha_N d_N) + 2Y_N Y_1 t(\alpha_N d_N C_N - S_N)\}. \tag{17}$$

The electric field associated to the surface modes of the semi-infinite $N$-layer superlattice [Eq. (10)] is given by[33]

$$E_i(n,x) \propto \frac{1}{S_i}\left[Y_i \sinh \alpha_i\left(\frac{d_i}{2} - x\right) + Y_{i+1} \sinh \alpha_i\left(\frac{d_i}{2} + x\right)\right]e^{inqD} i = 1,2,\cdots,N-1, \tag{18}$$

$$E_N(n,x) \propto \frac{1}{S_N}\left[Y_N \sinh \alpha_N\left(\frac{d_N}{2} - x\right) + tY_1 \sinh \alpha_N\left(\frac{d_N}{2} + x\right)\right]e^{inqD}. \tag{19}$$

## III. NUMERICAL AND EXPERIMENTAL RESULTS

### A. Bulk modes

Figure 3(a) shows the allowed and prohibited frequencies (distribution of the bandwidths) of a Fibonacci superlattice versus the generation number $k$ going until the eighth generation (34 blocks). Higher generations are shown in Fig. 3(b) for frequencies around the center of the spectrum. In Fig. 3, the limits of the bulk bands are given by $QD=0$ and $QD=\pi$ in Eq. (5) in such a way that one has an alternation from one band to another according to the sequence $0,\pi,\pi,0,0,\pi,\pi,0,\ldots$. The number of the allowed bands is equal to the number of blocks $F_k$ in each generation for $f<100$ MHz. Actually, it is sufficient to discuss the band structure of the Fibonacci structure in the frequency range $f<100$ MHz. Indeed, with our choice of the lengths of the cables ($d=1$ m), the whole spectrum of the Fibonacci structure is repeated periodically every $\frac{\omega d\sqrt{\varepsilon}}{c}=\pi$ (i.e., $f\simeq 98.68$ MHz). One can notice that, as expected, the allowed bands become narrower as far as $k$ increases, showing the localized character of the modes. Indeed, we have calculated the total width $\Delta_k$ of the allowed bands and shown that

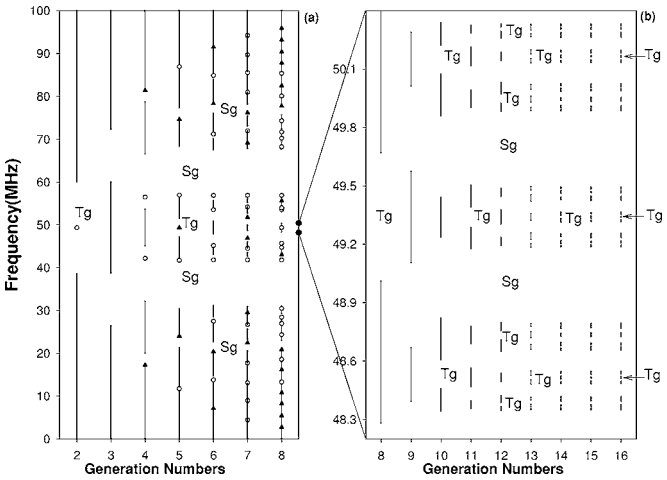


FIG. 3. (a) Distribution of the bandwidths (vertical lines) as a function of the generation number. $T_g$ and $S_g$ indicate the positions of transient and stable gaps, respectively. Open circles and full triangles correspond to the surface modes of two complementary superlattices *RSL* and *LSL* [Fig. 2(b)], respectively (see discussion in the text). (b) Same as (a) but for high generations in the frequency range [48.2,50.4] MHz around the central frequency $f_c=49.34$ MHZ in order to show the positions of the transient gaps ($T_g$) around $f_c$ which appear every three generations.

it is connected to the number of blocks $F_k$ for each generation $k$ according to the power law

$$\Delta_k = F_k^{-\delta}, \tag{20}$$

with $\delta\simeq 0.137$. For higher values of $k$, $\Delta_k$ (the Lebesgue measure of the energy bands) tends towards zero, consequently all the states become critical. This result, specific to quasiperiodic structures, was found in other types of excitations such as phonons or magnons.[18] One can also notice in Fig. 3(a), the existence of stable gaps around $f=22$, 35, 65, and 78 MHz (labeled $S_g$), which appear for all the generation numbers and transient gaps (labeled $T_g$) around the central frequency $f_c=\frac{\omega d\sqrt{\varepsilon}}{c}=\frac{\pi}{2}$ (i.e., $f_c=49.34$ MHz) for $S_2,S_5,S_8,\ldots$,[35] which appear every three generations. This is illustrated in Fig. 3(b) where a large zoom of the bandwidths around $f_c$ up to the 16th generation is sketched. In Figs. 3(a) and 3(b), one can notice that the width of the stable gaps remains almost constant for all generation numbers, while the width of the transient gaps decreases as the number of generations increases. However, the widths of all these gaps increase leading to a decreasing of the bulk bands widths following the power law [Eq. (20)].

In order to show experimentally the bulk band fragmentation versus the generation numbers, we measured the transmission spectrum through finite periodic structures placed between two semi-infinite waveguides[34] for different generations. Figure 4 represents the theoretical (solid line) and experimental (open circles) transmission spectra for a periodic Fibonacci structure made up of four cells. Each cell corresponds to sequences $S_2$, $S_3$, $S_4$, and $S_5$. The horizontal solid lines correspond to the bulk bands of an infinite periodic Fibonacci structure. The transmission measurements have

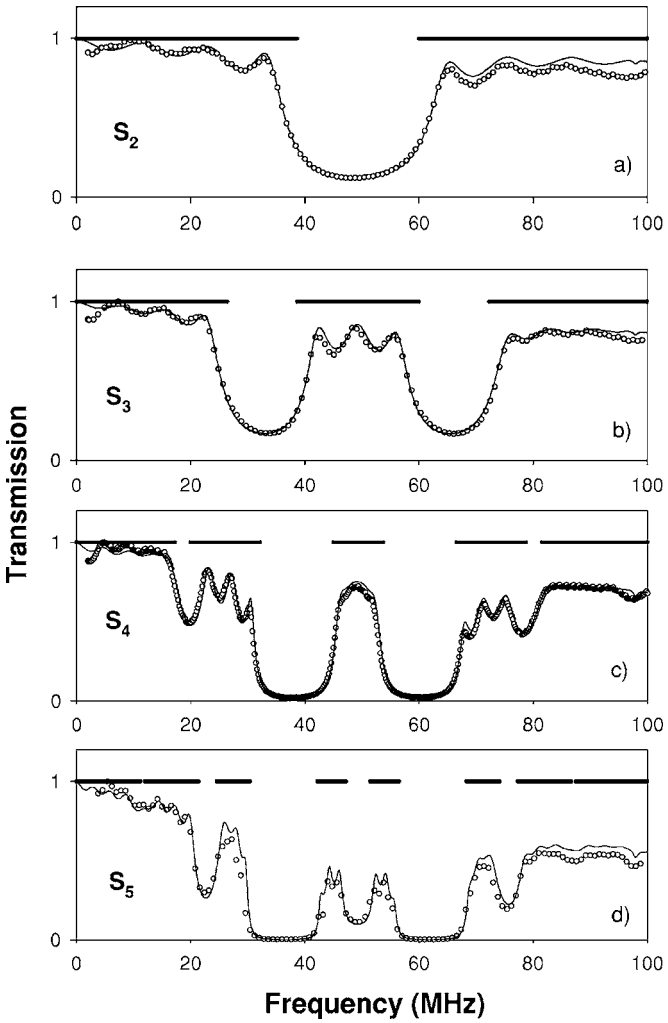


FIG. 4. Transmission spectrum as a function of the frequency for a finite periodic structure made up of four cells. Each cell is a Fibonacci generation $S_k$ $(k=2,3,4,5)$. Solid lines and open circles represent theoretical and experimental results, respectively. The horizontal lines correspond to the bandwidths of the infinite superlattices [Fig. 3(a)].

been realized by using the tracking generator coupled to a spectrum analyzer in the frequency range up to 100 MHz. The attenuation inside the coaxial cables was simulated by introducing a complex relative dielectric permittivity $(\varepsilon=\varepsilon' - j\varepsilon'')$. The attenuation coefficient $\alpha''$ can be expressed as $\alpha''=\varepsilon''\omega/c$. On the other hand, the attenuation specification data supplied by the manufacturer of the coaxial cables in the frequency range up to 100 MHz can be approximately fitted with the expression $\ln(\alpha'')=a+b\ln(\omega)$, where $a$ and $b$ are two constants. From this fitting procedure, a useful expression for $\varepsilon''$ as a function of frequency can be obtained under the form $\varepsilon''=0.017f^{-0.5}$ where the frequency $f$ is expressed in Hertz. The experimental results are very well fitted by the 1D model using the Green's function method. The results in Fig. 4 clearly show the fragmentation of the spectrum (subdivision of the bands) when one goes from a Fibonacci generation to a higher generation. Despite of the low number of cells (four) used in the finite structure, the transmission spectra describe very well the band structure of the infinite system. The attenuation effect in coaxial cables induces a transmission depletion, particularly at high frequencies. Also, this effect limits the study of high generation structures where the small gaps are not well-defined in the transmission spectra [see Fig. 4(d)]. For this reason, it is difficult to give an experimental verification of the power law [Eq. (20)] property of the Fibonacci structures studied here.

### B. Surface modes: Numerical results

Some years ago, El Boudouti *et al.*[33] have shown theoretically in the case of the transverse elastic waves that the creation of two semi-infinite superlattices from an infinite N-layer superlattice enables the creation of one surface mode by gap for any value of the wave vector parallel to the interfaces. This result was confirmed experimentally in a two-layer metallic superlattice Ag/Al.[36] Recently, Djafari-Rouhani *et al.*[29] confirmed these results in a comb-like photonic structure made out by resonators grafted periodically along a guide. In this section, we present an extension of this work to the case of a semi-infinite Fibonacci superlattice. In particular, as in our previous works, we consider two complementary semi-infinite superlattices obtained by the cleavage of an infinite superlattice [Fig. 2(b)]. One can notice that when one goes from generation to generation, the surface terminations of these two superlattices do not behave in the same way. For example, the cleavage of an infinite superlattice corresponding to the fourth Fibonacci generation $\ldots|ABAAB|ABAAB|ABAAB|ABAAB|\ldots$. gives rise to what we have called *LSL* and *RSL* semi-infinite superlattices:

$$\ldots|ABAAB|ABAAB| \quad \text{and} \quad |ABAAB|ABAAB|\ldots . \tag{21}$$

In the same way, one obtains for the fifth Fibonacci generation:

$$\ldots|ABAABABA|ABAABABA| \quad \text{and}$$
$$|ABAABABA|ABAABABA|\ldots . \tag{22}$$

These results show that the terminations of the *RSL* remain unchanged, whereas, the terminations of the *LSL* change from generation to generation. However, the *LSL* terminations remain similar for even generations (with block *B* at the surface) and odd generations (with block *A* at the surface).

In Fig. 3(a), we represented the surface modes for two complementary semi-infinite superlattices for various generations until the eighth generation. The open circles give the surface modes of the *RSL* and the full triangles those of the complementary *LSL*. These modes are obtained from the dispersion relation [Eqs. (10) and (11)]. One can notice the existence of one surface mode per gap, this mode is associated with the surface of one of the two semi-infinite periodic structures. To explain the origin of this result, we illustrated in Fig. 5 the variation of the density of states between the semi-infinite superlattice and the same volume of an infinite superlattice [Eqs. (16) and (17)] for both superlattices *RSL* [Fig. 5(a)] and *LSL* [Fig. 5(b)] corresponding to the fourth generation. The localized surface modes appear as delta peaks of weight unity. These peaks are enlarged artificially

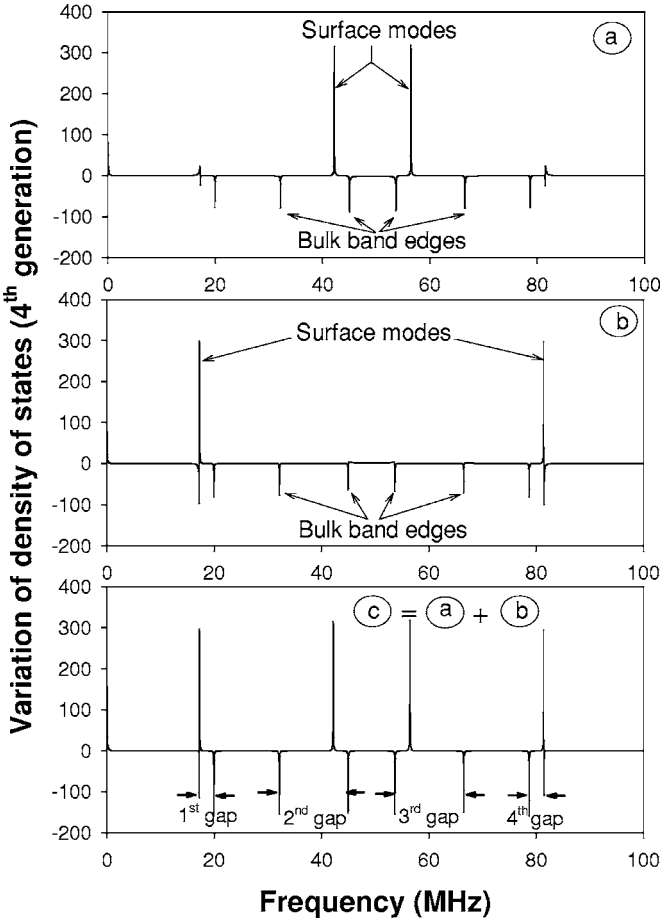


FIG. 5. (a) Variation of the total density of states (in arbitrary unit) between the semi-infinite superlattice *RSL* [Fig. 2(b)] and the same volume of the infinite superlattice [Fig. 2(a)] as a function of the frequency for the fourth generation. Positive $\delta$ peaks indicate the positions of surface modes, while the negative $-\frac{1}{4}\delta$ peaks correspond to the limits of the bulk bands. (b) Same as (a) for the *LSL* superlattice. (c) Same as (a), but for the two complementary superlattices.

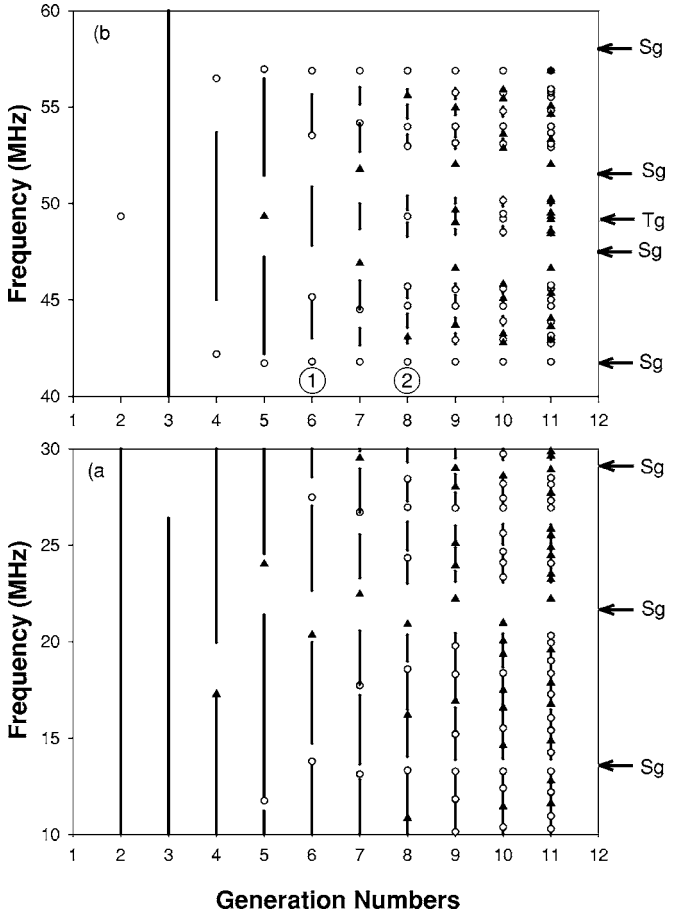


FIG. 6. Same as in Fig. 3, but enlarged in the range of frequencies [10, 30] MHz (a) and [40 ,60] MHz (b) in order to illustrate clearly the positions of the different surface modes in the stable and transient gaps. The positions of these gaps are indicated by arrows on the right side of these curves.

by adding a small imaginary part to the frequency $\omega$. At the bulk band edges appear delta peaks of weight $-\frac{1}{4}$, these peaks do not display exactly the same weight because of the divergences which exist at the bulk band edges in the density of states of 1D systems. Now, when one considers together the two complementary superlattices [Fig. 5(c)]: (i) the variation of density of states presents a loss of one half-mode at the limit of each band, i.e., one mode by band. (ii) The variation of density of states vanishes inside the bulk bands of the two complementary structures. These two results associated with the necessary conservation of the total number of modes show that a surface mode of weight unity by gap must exist [Fig. 5(c)] to compensate the loss of one mode by band. It is worth noticing that the analytical expression giving the frequencies of the surface modes for two complementary semi-infinite superlattices [Eq. (10)] is exactly the same as that giving the standing waves of one unit cell with free surfaces.[33] In Fig. 3(a), one can distinguish two types of surface modes.

(i) The modes falling inside the stable gaps. These modes appear almost at the same frequency for all the generations of the *RSL* (open circles) and for one generation over two of the *LSL* (full triangles). This result is understandable since, as mentioned above, the terminations of the *RSL* remain unchanged as a function of the generation number, while the terminations of the *LSL* changes in an alternating way for even and odd generations. This result is well illustrated in Fig. 6 where we have magnified Fig. 3 in the frequency intervals [10,30] MHz [Fig. 6(a)] and [40,60] MHz [Fig. 6(b)] and going until the 11th generation. Let us notice that the frequency region [70,90] MHz is equivalent to [10,30] MHz since the frequency spectrum of Fig. 3(a) is symmetrical around the central frequency $f_c$. Let us mention that similar results were found for magnetostatic modes in Fibonacci structures made of magnetic and nonmagnetic layers.[37]

(ii) The modes falling inside the transient gaps around $f_c$ [Fig. 3(b)]. These modes appear at the same frequency each six generations according to the splitting pattern presented in Fig. 7 for the *RSL*. It is seen that one "central" frequency is formed after six generations out of which two surface modes are formed in the transient gaps [Fig. 3(b)] after two genera-

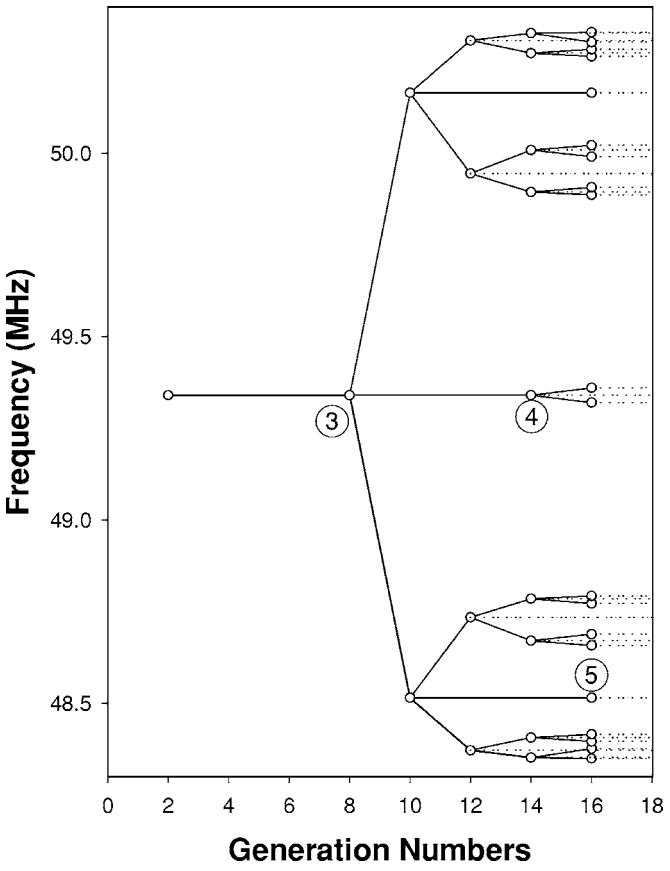


FIG. 7. Splitting pattern of surface modes inside the transient gaps of Fig. 3 for the *RSL* superlattice around the central frequency $f_c$=49.34 MHz (i.e., $\frac{\omega d\sqrt{\varepsilon}}{c}=\pi/2$).

tions. Then the splitting pattern repeats. The same diagram is obtained for the *LSL* where a surface mode appears between two surface modes of the same frequency of the *RSL*.

An analysis of the electric field or equivalently the local density of states (Fig. 8), enables us to study the spatial localization of the two types of surface modes discussed above. The localization length is defined as $\ell=\frac{1}{|\chi|}$ where $\chi$ is the imaginary part of the wave vector $Q$ obtained from Eq. (5). The surface modes falling inside the stable gaps present almost the same localization length (~8 m), as it is illustrated in Figs. 8(a) and 8(b) for the modes labeled 1 and 2 in Fig. 6(b) for the generations $S_6$ and $S_8$, respectively. On the other hand, the modes inside the transient gaps present a localization length proportional to the period $D$. Indeed, one can show analytically that $\ell=D/\log 2$ for the modes falling at the central frequency $f_c$=98.34 MHz. The same expression was found also by Zijlstra *et al.*[38] for surface states in Fibonacci superlattices using a tight binding model. We check numerically that this value remains almost the same for the surface modes in the transient gaps lying at the vicinity of $f_c$ (Fig. 7). This result shows that, contrary to the modes in the stable gaps, the localization length of the modes in the transient gaps increases with the generation number as it is illustrated in Figs. 8(c) and 8(d) for the modes labeled 3 and 4 in Fig. 7 for $S_8$ and $S_{14}$, respectively. The spatial localization of the two types of surface modes discussed above present different behaviors as a function of the space position $x$. The surface modes in the stable gaps decrease from the surface while penetrating into the bulk of the superlattice [Figs. 8(a) and 8(b)] as in ordinary periodic superlattices. However, the modes in the transient gaps present an important localization at the middle of each cell and a self-similar behavior of order six [see Figs. 8(c) and 8(d) for $S_8$ and $S_{14}$, respectively]. These results show that the electric field around the central frequency is neither extended nor localized. These spectra, which are due to the quasiperiodicity of the blocks $A$ and $B$ inside each unit cell, can be characterized by the multifractal analysis. This concept has been successfully used to understand the critical wave functions in the Fibonacci tight binding model[39] and $k$-component Fibonacci quantum waveguide.[40] However, as far as we know, this concept has not been applied for localized surface modes lying in the transient gaps.

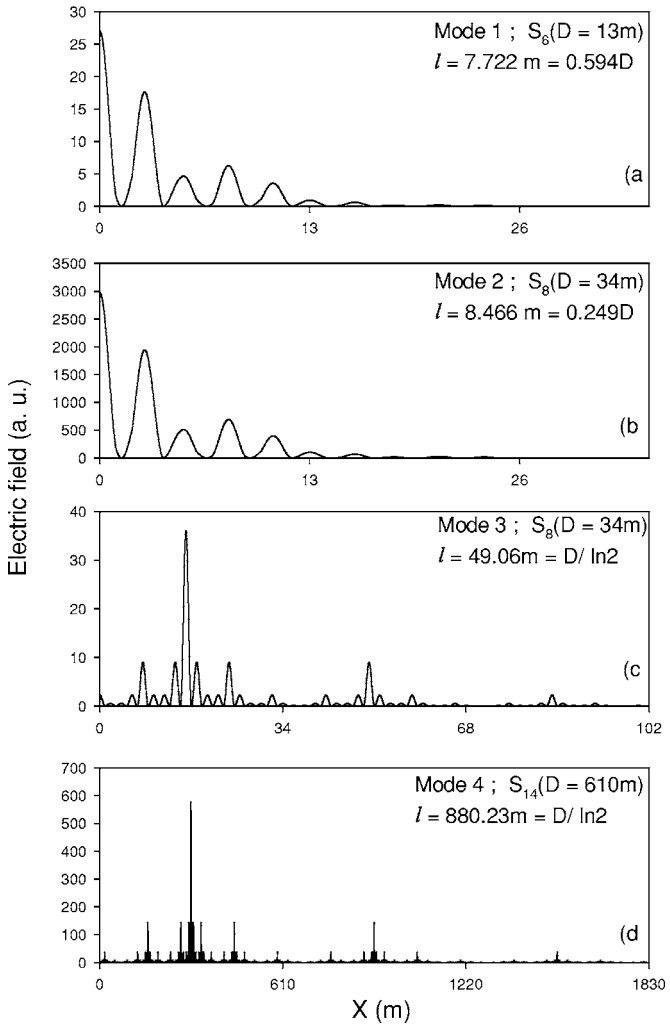


FIG. 8. (a) and (b) Modulus of the electric field as a function of the space position for the modes labeled 1 and 2 in Fig. 6, respectively. (c) and (d) Same as in (a) and (b) for the modes labeled 3 and 4 in Fig. 7, respectively.

The multifractal analysis enables us to describe the statistical properties of measure. If one covers the support of the measure by a partition of boxes of size $\varepsilon$ and one denotes by

$p_i(\varepsilon)$ the probability (integrated measure) in the $i$th box, an exponent (singularity strength) $\alpha_i$ can be defined as

$$p_i(\varepsilon) \simeq \varepsilon^{\alpha_i}. \tag{23}$$

If we count the number of boxes $N(\alpha)d\alpha$ where the probability $p_i$ has singularity strength between $\alpha$ and $\alpha+d\alpha$, then $f(\alpha)$ can be defined as the fractal dimension of the whole set of boxes of singularity strength $\alpha$ as

$$N(\alpha)d\alpha \sim \varepsilon^{-f(\alpha)}d\alpha. \tag{24}$$

Several models based on the calculation of the generalized fractal dimension $D_q$ were elaborated[41–43] to calculate $\alpha$ and $f(\alpha)$ using a Legendre transform. However, the application of this method presents several difficulties with the Legendre transform itself in particular when $f(\alpha)$ exhibit discontinuities.[44] To solve this problem, a new precise mathematical method was proposed by Chabra *et al.*[45] It allows the calculation of $f(\alpha)$ with an excellent numerical precision. This method was applied successfully for several elementary excitations in 1D systems,[18,40] and it is the method used here. In this method, the first step in multifractal characterization is the probability measure $p_i$. In our case, we choose the probability $p_i$ as the weight of the electric field in the density spectrum, i.e.,

$$p_i = \frac{|E_i|^2}{\sum_{j=1}^{N} |E_j|^2}, \tag{25}$$

where $N=F_k$ is the total number of blocks considered in one cell of the generation $k$ and $|E_i|$ is the mean electric field in the block $i$. Then, we construct a partition function:

$$Z(q) = \sum_{i=1}^{N} p_i^q, \tag{26}$$

where the parameter $q$ provides a microscope for exploring the singular measure in different regions. The mulifractal spectrum $f(\alpha)$ is obtained by varying the parameter $q$ in Eq. (26) and calculating[40]

$$\alpha = -\frac{1}{\log N}\frac{Z'(q)}{Z(q)}, \tag{27}$$

$$f(\alpha) = \frac{1}{\log N}\left[\log Z(q) - q\frac{Z'(q)}{Z(q)}\right] \tag{28}$$

with

$$Z'(q) = \frac{dZ}{dq} = \sum_{i=1}^{N} p_i^q \log p_i.$$

The $f(\alpha)$ singularity spectrum gives a precise description of the distribution of the electric field in the structure. Indeed, it is well established[39] that $f(\alpha)$ is reduced to a single point $f(\alpha=1)=1$ for extended modes and $f(\alpha=0)=0$ and $f(\alpha=\infty)=1$ for localized modes. However, for self-similar modes, $f(\alpha)$ is expected to have a smooth function defined in a finite region $[\alpha_{min}, \alpha_{max}]$.

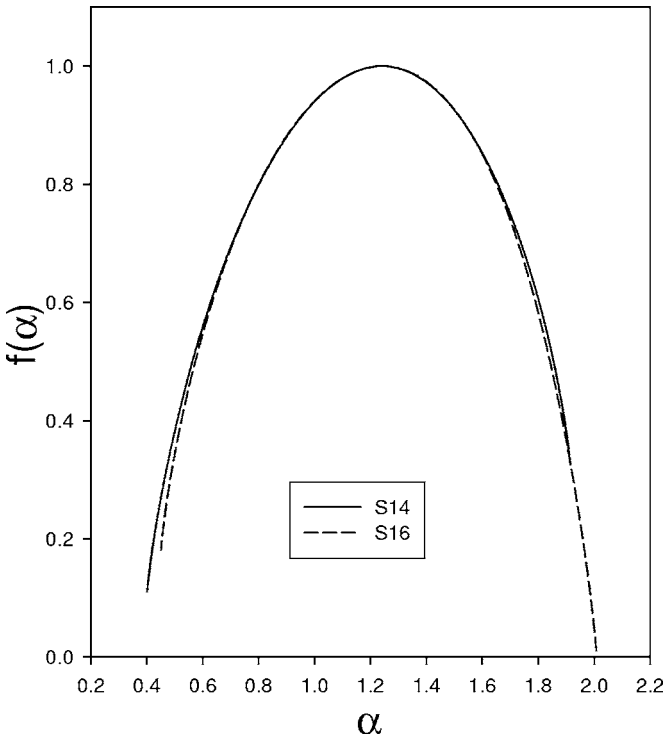


FIG. 9. The $f(\alpha)$ curve for the distribution of the modulus of the electric field corresponding to the modes labeled 4 (solid line) and 5 (dashed line) in Fig. 7. The generations of these modes are 14th and 16th, respectively.

The numerical results of $f(\alpha)$ for the electric field associated to the modes labeled 4 and 5 in Fig. 7 are sketched in Fig. 9. These results clearly show that the modes lying in the transient gaps are neither extended nor localized but possess multifractal properties which are characteristic of self-similar modes. In Fig. 9, $\alpha_{min}$ and $\alpha_{max}$ characterize the scaling property of the most concentrated and most rarefied regions of the density measure respectively.[18] The quantity $\Delta_\alpha=\alpha_{max}-\alpha_{min}$ can be used as a parameter reflecting the randomness of the intensity measure. Contrary to localized modes lying in transient gaps, the electric field associated to surface modes lying in the stable gaps [Figs. 8(a) and 8(b)] exhibit

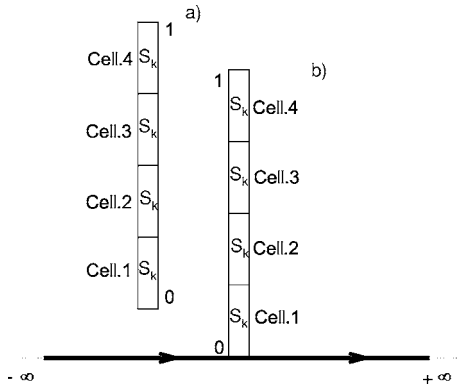


FIG. 10. (a) Finite superlattice made up of four cells, each cell is a Fibonacci generation $S_k$. (b) Finite superlattice attached vertically to a horizontal guide.

the property of localized waves, namely $\alpha_{min} \simeq 0$ and $\alpha_{max}$ increases rapidly with the increasing generation number.

### C. Surface modes: Experimental results

In order to give experimental evidence of the existence of surface modes in Fibonacci superlattices, we propose a method that consists of vertically attaching a finite periodic Fibonacci structure to a horizontal waveguide (Fig. 10). Indeed, the transmission coefficient through such a structure may give us information on all the eigenmodes of the finite structure with free surfaces. Let $g^{-1}(MM)$ be the inverse of the Green function of the finite structure in the space of the interfaces $M=\{0,1\}$ [Fig. 10(a)]. $g^{-1}(MM)$ can be written in the form:

$$g^{-1}(MM) = \begin{pmatrix} g^{-1}(0,0) & g^{-1}(0,1) \\ g^{-1}(1,0) & g^{-1}(1,1) \end{pmatrix}. \tag{29}$$

If one grafts vertically this structure to two semi-infinite waveguides of impedances $Z_s$ on the site $\{0\}$ [Fig. 10(b)], one obtains the Green function of the final system on this site as follows:[29,34]

$$d(0,0) = \frac{g^{-1}(1,1)}{[g^{-1}(0,0)g^{-1}(1,1) - g^{-1}(0,1)g^{-1}(1,0)] - 2jg^{-1}(1,1)/Z_s}. \tag{30}$$

The site $\{0\}$ is the point where it is carried out the reflection and the transmission of an incident wave launched from the left semi-infinite waveguide $(-\infty,0)$ [Fig. 10(b)]. The transmitted wave in the right semi-infinite waveguide $(0,+\infty)$ is given by

$$t = \frac{-2jg^{-1}(1,1)/Z_s}{[g^{-1}(0,0)g^{-1}(1,1) - g^{-1}(0,1)g^{-1}(1,0)] - 2jg^{-1}(1,1)/Z_s}. \tag{31}$$

The eigenmodes of the finite structure with free surfaces [Fig. 10(a)] are given by $\det g^{-1}(MM) = g^{-1}(0,0)g^{-1}(1,1) - g^{-1}(0,1)g^{-1}(1,0) = 0$ [Eq. (29)]. Consequently, the transmission coefficient [Eq. (31)] becomes equal to unity. This result shows that all the eigenmodes of the finite structure can be obtained from the maxima of the transmission coefficient of the same structure grafted vertically on a horizontal guide. Some transmission spectra for the generations $S_3$ and $S_4$ corresponding to one and four grafted cells are presented in Fig. 11. Theoretical results (solid lines) are in good agreement with experimental curves (open circles). As mentioned before, these curves present minima and maxima. The frequencies corresponding to the maxima of these curves give the eigenmodes of the finite structure with free surfaces. These modes are shown by small horizontal lines and open circles in Fig. 12(a) for one and four cells, respectively, in each generation. The vertical solid lines represent the bulk bands of the infinite structure [Fig. 3(a)]. One can notice that the eigenmodes of one cell with free surfaces falling inside the forbidden bands of the superlattice coincide with the surface modes of two complementary semi-infinite superlattices [Fig. 3(a)]. These experimental results confirm the theoretical results shown in Ref. 33 and recalled in Sec. II A, namely the standing modes of one cell with free surfaces and falling inside the forbidden bands of the infinite superlattice are exactly the surface modes of two complementary semi-infinite superlattices. In the case of four cells, one obtains besides the surface modes falling in the gaps, four modes in each band corresponding to the four cells constituting the finite struc-

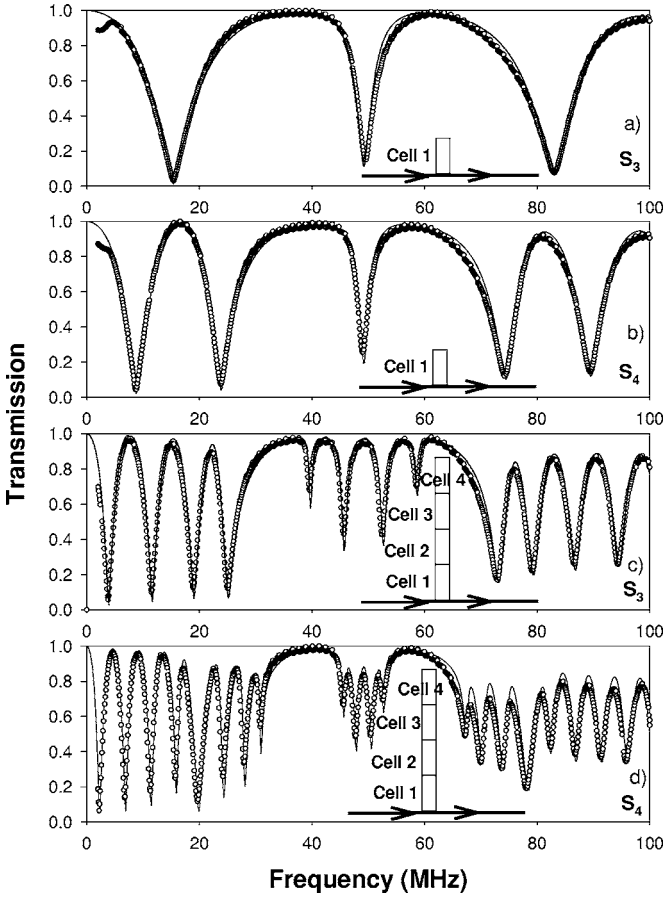


FIG. 11. Transmission spectrum of a finite periodic structure grafted vertically to a guide. The finite structure is made up of one, (a) and (b), and four, (c) and (d), cells. The blocks $A$ and $B$ in the unit cell respect the Fibonacci generation $S_k$ $(k=3,4)$.

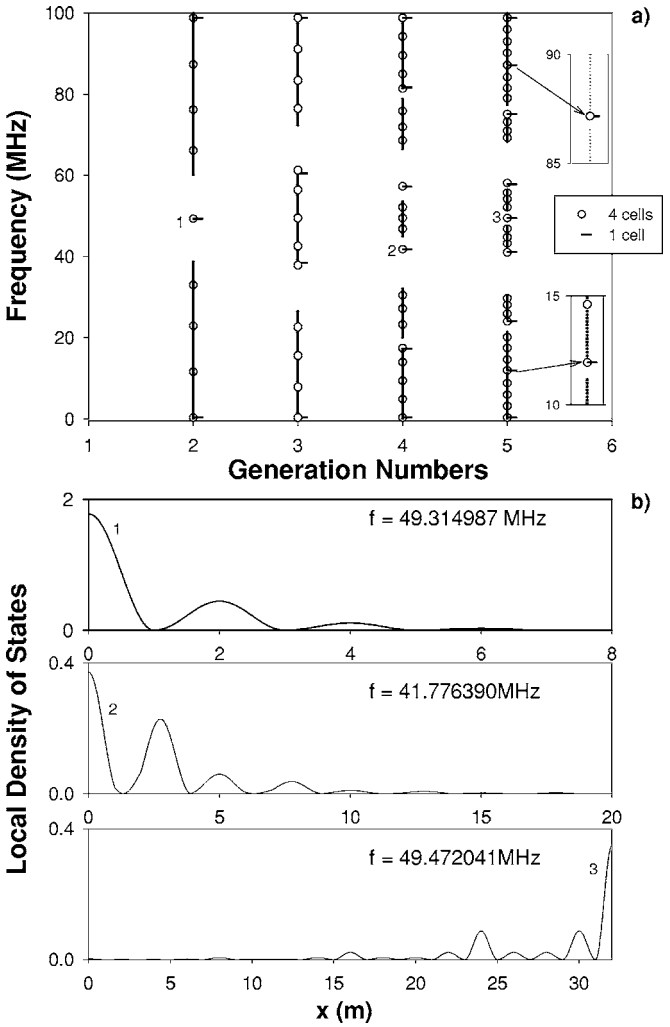


FIG. 12. (a) Same as in Fig. 3(a). The small horizontal lines represent the eigenmodes of the finite structure (one cell) obtained from the maxima of the transmission spectra. The open circles represent the modes corresponding to four cells instead of one. (b) Analysis of the local density of states as a function of the space position enables one to distinguish between the modes associated to the two surfaces of the finite structure. For example, the modes labeled 1 and 2 in Fig. 12(a) are associated with the surface grafted on the guide, while mode 3 is associated with the other free surface.

ture. These results show again the fragmentation of the bands when the generation number increases. An analysis of the local density of states as a function of the space position [Fig. 12(b)] enables us to distinguish the modes associated with the surrounding surfaces of the finite structure. For example, in the case of four cells, the modes labeled 1 and 2 [Fig. 12(a)] are associated with the surface grafted on the guide, while the mode 3 is associated to the other free surface. Despite the small number of cells (four), the spatial localization of the surface modes is analogous to that of surface modes in semi-infinite superlattices.

## IV. SUMMARY AND CONCLUSION

In this paper, we have presented theoretical results of bulk and surface electromagnetic modes in 1D quasiperiodic superlattices of Fibonacci type. The blocks *A* and *B* constituting these structures are formed by coaxial cables in the shape of loops and segments. Different properties related to the bulk bands such as the fragmentation of the frequency spectrum and the power law are analyzed and discussed. We generalize a theoretical rule on the existence of surface modes in the quasiperiodic superlattices, namely when one considers two semi-infinite superlattices obtained by the cleavage of an infinite superlattice, one obtains as many surface modes as minis-gaps. Two types of surface modes are found.

(i) The modes inside the stable gaps. These modes fall at the same frequency for the superlattice having its surface termination unchanged every generation. However, the surface modes of the complementary superlattice fall at two different stable frequencies as their terminations are not the same for odd and even generations. These modes are very localized at the surface and present almost the same localization length. They are related to the periodicity of the structure.

(ii) The modes inside the transient gaps. These modes appear each six-generations following a well-defined profile (Fig. 7) and their spatial localization shows the properties of self-similarity of order six and multifractality which are related to the quasiperiodicity of the structure.

Experimentally, we have shown the existence of the allowed and prohibited bands in Fibonacci superlattices by measuring the transmission through a finite periodic structure embedded horizontally between two semi-infinite waveguides. Moreover, we have proposed an original method to detect the surface modes by measuring the transmission through a guide along which the finite structure is attached vertically. Because of the absorption in the cables, we did not give an experimental verification of all the theoretical results in particular for high generations. However, for small generations below the fifth generation, the experimental results agree very well with the theoretical predictions. Finally, let us mention that our theoretical model can be applied to the study of other quasiperiodic structures such as Cantor, Thue-Morse, and double period.[18] Even though these structures present different band gap structures,[18] one can expect similar results to those presented here about surface modes, namely the existence of one surface mode per gap for two complementary semi-infinite superlattices as well as the different localization properties of surface modes in stable gaps and transient gaps.

## ACKNOWLEDGMENTS

E. H. E. gratefully acknowledges the hospitality of the UFR de Physique, Université de Lille 1. This work was supported by "Le Fond Européen de Développement Régional (FEDER), INTERREG III France-Wallonie-Flandre (PREMIO)" and "Le Conseil Régional Nord-Pas de Calais." The work of V. R. V. has been partially supported by the Ministerio de Educación y Ciencia (Spain) through Grant No. MAT2003-04278.

*Corresponding author. Electronic address: boudouti@sciences.univ-oujda.ac.ma

[1] See, for example, J. D. Joannopoulos, R. D. Meade, and J. N. Winn, *Photonic Crystals* (Princeton University Press, Princeton, NJ, 1995); *Photonic Band Gap and Localization*, edited by C. M. Soukoulis (Plenum, New York, 1993); *Photonic Band Gap Materials*, edited by C. M. Soukoulis (Kluwer, Dordrecht, 1996).

[2] S. Johnson and J. D. Joannopoulos, *Photonic Crystals: The Road from Theory to Practice* (Kluwer Academic Publishers, Boston, 2002).

[3] J. C. Knight, J. Broeng, T. A. Birks, and P. St. J. Russell, Science **282**, 1476 (1998).

[4] R. D. Meade, K. D. Brommer, A. M. Rappe, and J. D. Joannopoulos, Phys. Rev. B **44**, 10961 (1991).

[5] W. M. Robertson, G. Arjavalingam, R. D. Meade, K. D. Brommer, A. M. Rappe, and J. D. Joannopoulos, Opt. Lett. **18**, 528 (1993).

[6] F. Ramos-Mendieta and P. Halevi, Solid State Commun. **100**, 314 (1996); F. Ramos-Mendieta and P. Halevi, Phys. Rev. B **59**, 15112 (1999).

[7] P. Yeh, A. Yariv, and C. S. Hong, J. Opt. Soc. Am. **67**, 423 (1977).

[8] N. Ng, P. Yeh, and A. Yariv, Appl. Phys. Lett. **32**, 370 (1978).

[9] A. A. Bulgakov and V. R. Koturn, Opt. Spectrosc. **56**, 269 (1984).

[10] W. M. Robertson and M. S. May, Appl. Phys. Lett. **74**, 1800 (1999).

[11] F. Ramos-Mendieta and P. Halevi, J. Opt. Soc. Am. B **14**, 370 (1997).

[12] M. L. H. Lahlaouti, A. Akjouj, B. Djafari-Rouhani, L. Dobrzynski, M. Hammouchi, E. H. El Boudouti, A. Nougaoui, and B. Kharbouch, Phys. Rev. B **63**, 035312 (2001).

[13] F. Villa, J. A. Gaspar-Armenta, and F. Ramos-Mendieta, Opt. Commun. **216**, 361 (2003).

[14] S. Feng, H-Yi. Sang, Z-Y. Li, B-Y. Cheng, and D-Z. Zhang, J. Opt. A, Pure Appl. Opt. **7**, 374 (2005).

[15] D. N. Chigrin, A. V. Lavrinenko, D. A. Yarotsky, and V. Gaponenko, J. Lightwave Technol. **17**, 2018 (1999).

[16] T. Okamoto, T. Kamiyama, and I. Yamaguchi, Opt. Lett. **18**, 1570 (1993).

[17] W. M. Robertson, J. Lightwave Technol. **17**, 2013 (1999).

[18] E. L. Albuquerque and M. G. Cottam, Phys. Rep. **376**, 225 (2003); *Polaritons in Periodic and Quasiperiodic Structures* (Elsevier, Amsterdam, 2004).

[19] M. Kohmoto, B. Sutherland, and K. Iguchi, Phys. Rev. Lett. **58**, 2436 (1987).

[20] W. Gellermann, M. Kohmoto, B. Sutherland, and P. C. Taylor, Phys. Rev. Lett. **72**, 633 (1994).

[21] T. Hattori, N. Tsurumachi, S. Kawato, and H. Nakatsuka, Phys. Rev. B **50**, R4220 (1994).

[22] L. Chow and K. H. Guenther, J. Opt. Soc. Am. A **10**, 2231 (1993).

[23] R. Pelster, V. Gasparian, and G. Nimtz, Phys. Rev. E **55**, 7645 (1997).

[24] R. W. Peng, Y. M. Liu, X. Q. Huang, F. Qiu, Mu Wang, A. Hu, S. S. Jiang, D. Feng, L. Z. Ouyang and J. Zou, Phys. Rev. B **69**, 165109 (2004).

[25] M. Ghulinyan, C. J. Oton, L. D. Negro, L. Pavesi, R. Sapienza, M. Colocci, and D. S. Wiersma, Phys. Rev. B **71**, 094204 (2005).

[26] C. Sibilia, I. S. Nefedov, M. Scalora, and M. Bertolotti, J. Opt. Soc. Am. B **15**, 1947 (1998).

[27] X. Huang, Y. Wang, and C. Gong, J. Phys.: Condens. Matter **11**, 7645 (1999).

[28] E. Macia, Phys. Rev. B **63**, 205421 (2001).

[29] B. Djafari-Rouhani, E. H. El Boudouti, A. Akjouj, L. Dobrzynski, J. O. Vasseur, A. Mir, N. Fettouhi, and J. Zemmouri, Vacuum **63**, 177 (2001).

[30] E. H. El Boudouti, N. Fettouhi, A. Akjouj, B. Djafari-Rouhani, A. Mir, J. O. Vasseur, L. Dobrzynski, and J. Zemmouri, J. Appl. Phys. **95**, 1102 (2004).

[31] H. Aynaou, E. H. El Boudouti, Y. El Hassouani, A. Akjouj, B. Djafari-Rouhani, J. Vasseur, A. Benomar, and V. R. Velasco, Phys. Rev. E **72**, 056601 (2005).

[32] L. Dobrzynski, Surf. Sci. Rep. **11**, 139 (1990).

[33] E. H. El Boudouti, B. Djafari-Rouhani, A. Akjouj, and L. Dobrzynski, Phys. Rev. B **54**, 14728 (1996).

[34] J. Vasseur, A. Akjouj, B. Djafari-Rouhani, L. Dobrzynski, and E. H. El Boudouti, Surf. Sci. Rep. **51**, 1 (2004).

[35] F. Piechon, M. Benakli, and A. Jagannathan, Phys. Rev. Lett. **74**, 5248 (1995).

[36] W. Chen, Y. Lu, H. J. Maris, and G. Xiao, Phys. Rev. B **50**, 14506 (1994).

[37] J. W. Feng, G. J. Jin, A. Hu, S. S. Kang, S. S. Jiang, and D. Feng, Phys. Rev. B **52**, 15312 (1995).

[38] E. S. Zijlstra, A. Fasolino, and T. Janssen, Phys. Rev. B **59**, 302 (1999).

[39] T. Fujiwara, M. Kohmoto, and T. Tokihiro, Phys. Rev. B **40**, 7413 (1989)

[40] R. W. Peng, G. J. Jin, M. Wang, A. Hu, S. S. Jiang, and D. Feng, J. Phys.: Condens. Matter **12**, 5701 (2000).

[41] For a review, see J. L. McCauley, Phys. Rep. **189**, 225 (1990).

[42] T. C. Halsey, M. H. Jensen, L. P. Kadanoff, I. Procaccia, and B. I. Shraiman, Phys. Rev. A **33**, 1141 (1986).

[43] M. Kohmoto, B. Sutherland, and C. Tang, Phys. Rev. B **35**, 1020 (1987).

[44] P. Grassberger, R. Badii, and A. Politi, J. Stat. Phys. **51**, 135 (1988).

[45] A. Chhabra and R. V. Jensen, Phys. Rev. Lett. **62**, 1327 (1989).